

Observations of Transient Active Region Heating with Hinode

Harry P. WARREN¹, Ignacio UGARTE-URRA^{1,2}, David H. BROOKS^{1,2}, Jonathan W. CERTAIN³, David R. WILLIAMS⁴, and Hirohisa HARR

¹*Space Science Division, Naval Research Laboratory, Washington, DC 20375, USA*

²*College of Science, George Mason University, 4400 University Drive, Fairfax, VA 22030, USA*

³*Harvard-Smithsonian Center for Astrophysics, 60 Garden Street, Cambridge, MA 028138, USA*

⁴*Mullard Space Science Laboratory, University College London, Holmbury St Mary, Dorking, Surrey, RH5 6NT, UK*

⁵*National Astronomical Observatory of Japan, Mitaka, Tokyo, 181-8588*

hwarren@nrl.navy.mil, iugarte@ssd5.nrl.navy.mil

(Received (reception date); accepted (acceptation date))

Abstract

We present observations of transient active region heating events observed with the Extreme Ultraviolet Imaging Spectrometer (EIS) and X-ray Telescope (XRT) on Hinode. This initial investigation focuses on NOAA active region 10940 as observed by Hinode on February 1, 2007 between 12 and 19 UT. In these observations we find numerous examples of transient heating events within the active region. The high spatial resolution and broad temperature coverage of these instruments allows us to track the evolution of coronal plasma. The evolution of the emission observed with XRT and EIS during these events is generally consistent with loops that have been heated and are cooling. We have analyzed the most energetic heating event observed during this period, a small GOES B-class flare, in some detail and present some of the spectral signatures of the event, such as relative Doppler shifts at one of the loop footpoints and enhanced line widths during the rise phase of the event. While the analysis of these transient events has the potential to yield insights into the coronal heating mechanism, these observations do not rule out the possibility that there is a strong steady heating level in the active region. Detailed statistical analysis will be required to address this question definitively.

Key words: Sun: corona — Sun: activity

1. Introduction

Understanding how the solar corona is heated to high temperatures is one of the principal objectives of the Hinode mission (Kosugi et al. 2007). The Extreme Ultraviolet Imaging Spectrometer (EIS) on Hinode has an unprecedented combination of high spatial, spectral, and temporal resolution and provides a wealth of information on the temperatures, densities, velocities, and nonthermal motions in the solar corona. The X-ray Telescope (XRT) on Hinode is one of the highest spatial resolution soft X-ray telescopes ever built, and combines this high spatial resolution with high temporal resolution and a broad temperature coverage. Together, these instruments give us an unparalleled ability to probe the morphology and evolution of coronal plasma (see, Culhane et al. 2007 and Golub et al. 2007, for more details on the instruments).

One question of particular importance is the time scale for heating in solar active regions. Recent observations have yielded contradictory results. At high temperatures, observations at soft X-ray wavelengths have suggested that the emission is relatively steady and can be described with steady heating models. The analysis of individual loops (e.g., Porter & Klimchuk 1995; Kano & Tsuneta 1996) has shown that the evolution of the intensity is generally much slower than the conductive or radiative cooling times and that the loop emission is consistent with the RTV scaling laws (Rosner, Tucker, & Vaiana 1978). Transient brightenings have been observed in active regions previously (e.g., Shimizu et al. 1992), but they do not appear to provide sufficient heating (e.g., Shimizu

1995). The application of steady heating models to entire active regions (e.g., Warren & Winebarger 2006), coronal bright points (Brooks & Warren 2007), and the full Sun (Schrijver et al. 2004) have successfully reproduced the observed high temperature emission.

At lower temperatures, observations of active regions at temperatures near 1 MK suggest that coronal plasma is far from equilibrium. The analysis of coronal loops at these temperatures indicate very large densities relative to the RTV scaling laws (e.g., Winebarger et al. 2003; Aschwanden et al. 2001; Lenz et al. 1999). Full active region modeling shows that while the steady heating models can reproduce the high temperature emission, these models cannot account for the presence of cooler active region loops (Warren & Winebarger 2006). Because loops cool more rapidly than they drain (e.g., Cargill et al. 1995), impulsive heating models can account for the bright active region loop emission observed at these temperatures (e.g., Warren et al. 2002; Warren et al. 2003). Examples of active region loops cooling from high temperatures down through 1 MK have been documented (e.g., Winebarger & Warren 2005; Ugarte-Urra et al. 2006).

The different heating time scales suggested by the observations at different temperatures can be resolved in a number of ways. It may be that there is a different heating mechanism responsible for the plasma at different temperatures. Alternatively, it may be that high temperature emission is more dynamic than previously thought and the modest spatial resolution of previous instruments has obscured this. The purpose of this paper is to make an initial survey of some EIS and XRT

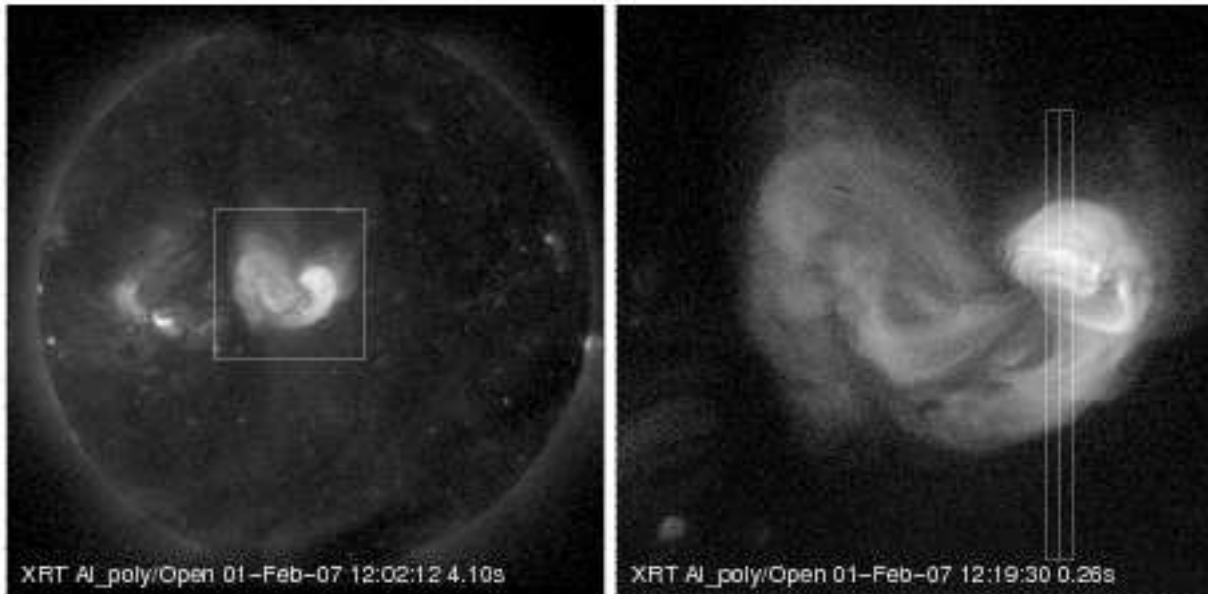


Fig. 1. XRT observations of AR 10940 on February 2, 2007. On the left is a composite full disk image. On the right is an example of a 512×512 pixel cutout. The field of view for the EIS context and sit-and-stare observations is indicated. A movie is provided as on-line material.

active region observations and to explore the available diagnostics.

2. Observations

NOAA active region 10940 traversed the solar disk observable from Earth from January 27 to February 10, 2007. In this paper we consider results from specially designed EIS active region observing sequences taken during the period February 1–6, 2007. The EIS observations during this period generally consisted of small context rasters ($40'' \times 400''$) used for co-alignment with XRT that were followed by a long series of exposures at a fixed position with the $1''$ slit taken at a cadence of 30 s. In both observing sequences 20 spectral windows 24 pixels wide and $400''$ long were selected to be included in the telemetry stream. These EIS sit-and-stare observations were typically run for periods of approximately 10 consecutive hours tracking a single position on the Sun.

Representative images from the XRT are shown in Figure 1. The XRT observations during this time generally consisted of 512×512 pixel cutouts at a cadence of about 60 s in the Al_{poly}/Open filter combination. XRT images in the Al_{poly}/Al_{thick} filter combination were taken at a cadence of about 360 s. Full disk synoptic observations in multiple filters were taken 4 times per day. Sample XRT images of this active region are shown in Figure 1.

3. Data Reduction

EIS spectra have been processed using current standard reduction software, which consists of CCD bias and dark current subtraction and cosmic ray and hot pixel removal. Pixels affected by the latter are flagged as missing and their values are replaced by the median value of the neighboring ones.

Spectral lines were fitted with single Gaussian profiles, ex-

cept for the Fe XIII doublet ($203.83/203.80 \text{ \AA}$) line which is a resolved blend with the Fe XII 203.73 \AA line. The fits return peak intensity, width, and center position of the line for every pixel along the slit and every exposure. Since the spacecraft tracks solar rotation in the sit-and-stare observations we obtain temporal variations of three parameters for the same position on the Sun.

The spectral information has to be corrected of two instrumental effects: the tilt of the slit on the CCD and the sinusoidal drift of the lines on the detector due to orbital changes. Further details and how to do the correction is given elsewhere (Mariska et al., this issue). Spatially, a North-South spacecraft drift is evident in the time slice intensity image of every line, i.e. the image that results from putting together in succession the intensity images of the slit for every exposure. This jitter is also present in the XRT movies, and can be corrected by cross-correlation of the XRT images with respect to a reference image, which was chosen to be the XRT image closest to the middle of the EIS context raster. The amplitudes of these offsets, which range from 1 to 4 XRT pixels, are used in first order to correct the spacecraft drift along the slit. The correction is satisfactory for the time series we have analyzed.

The co-alignment between XRT and EIS was established by cross-correlating the Al_{poly}/Open image taken closest to the middle of the EIS context raster in the Fe XVI 262.98 \AA line. For non-flaring active region conditions the morphology of the XRT Al_{poly}/Open images is very similar to the EIS Fe XVI 262.98 \AA raster.

From the location of the EIS slit on the co-aligned XRT datacube we extract a time slice, i.e. a Solar Y versus time image, that can be directly compared with the EIS time slices described above. The Al_{poly} XRT filter peak response is at around 8 MK, in the upper limit range of EIS temperature coverage, which makes it, apart from an excellent context image, a good complement in terms of temperature sampling.

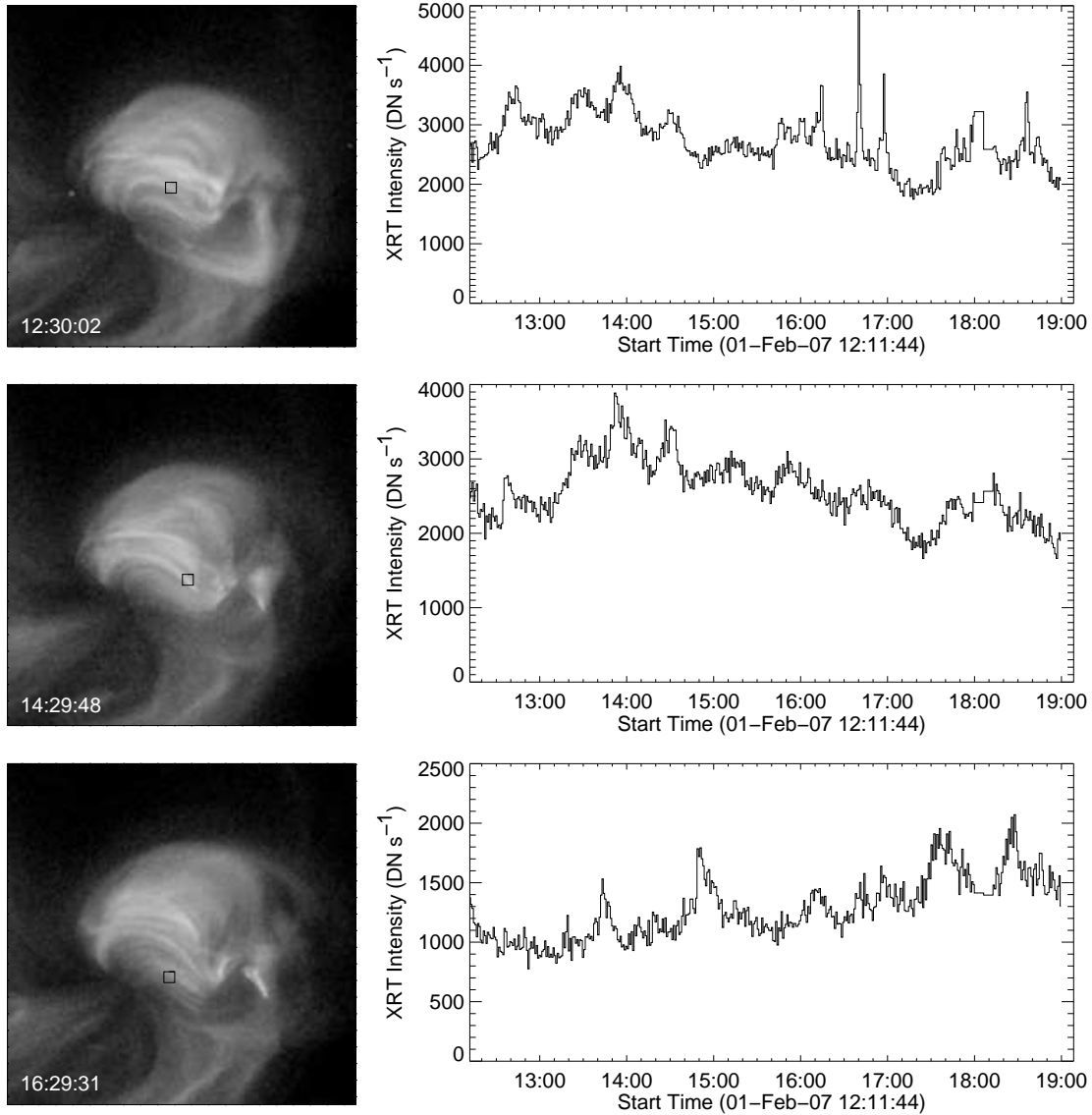


Fig. 2. Example XRT Al_{poly}/Open images and light curves for the bright emission in AR10940. The light curves are for single pixel locations and are indicated by the box on the corresponding image. We have not estimated the uncertainties in the XRT data but the intensity fluctuations in successive images give some indication of the noise level.

4. Results

XRT movies of this active region immediately reveal the dynamic nature of the high temperature emission. A wide variety of loops of different lengths and topological connections are observed to brighten up and disappear. Despite the rapid evolution of many loops within the active region, the general morphology of the active region is relatively constant, and the total intensity appears to evolve slowly.

To make these impressions more quantitative we have calculated light curves for individual pixels in the co-aligned XRT data cubes. As illustrated by the light curves shown in Figure 2, there are numerous pixels which show intensity variations of more than 100% during the course of the observations. The accompanying XRT images show that these intensity variations are related to brightenings in individual loops. The average intensity in the active region, in contrast, is much more steady,

varying by only $\pm 20\%$ during the 10 hours of observation.

To aid in the identification of events observed with EIS and XRT we have inspected stack plots of integrated line intensity as a function of time. We generally begin by identifying events in the XRT data and then look for the corresponding signatures in the EIS observations. We have found many examples of transient brightenings in these data. The general trend in the light curves supports the idea that these brightenings are heating events in individual loops. Intensity enhancements are usually first seen in the detector sensitive to hotter temperatures, the XRT Al_{poly} filter, and then in successively cooler emission lines: Fe XVI (2.5 MK), Fe XIV (2.0 MK), Fe XIII (1.6 MK), Fe XII and Si X (1.3 MK), and Si VII (0.6 MK). While this is the general trend there are many instances where the evolution of the plasma is confusing, presumably because of multiple structures along the line of sight.

For this initial study we focus on the brightest event that

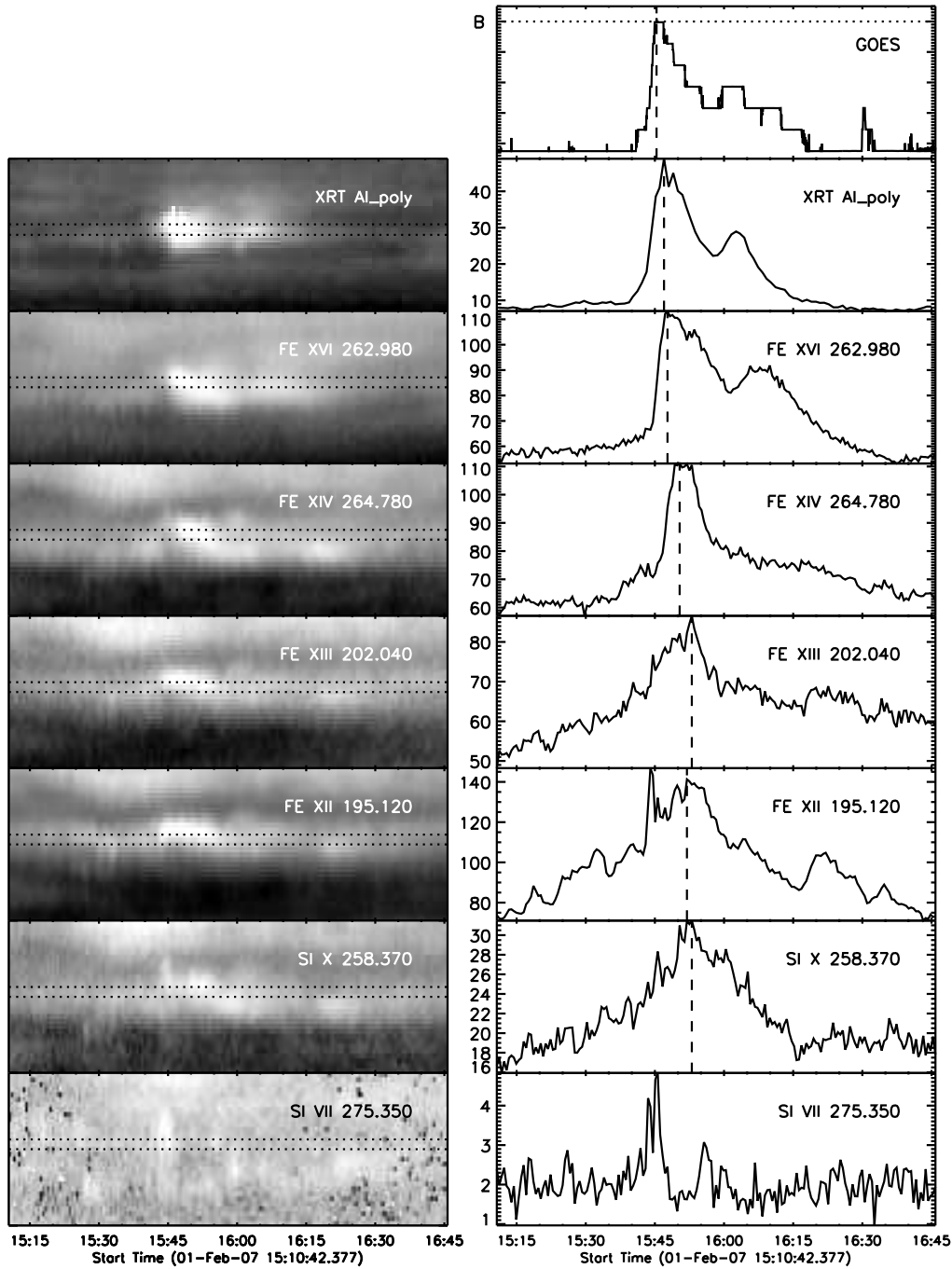


Fig. 3. Stack plots and light curves for a B flare observed on February 1, 2007 near 15:45 UT. On the left plots of intensity along the slit as a function of time are shown. On the right light curves are shown. The light curve has been computed from the three spatial pixels indicated by the dotted line. The dashed vertical line is the approximate position of the peak intensity. The units for the EIS intensities are $10^3 \text{ ergs cm}^{-2} \text{ s}^{-1} \text{ sr}^{-1}$. The XRT intensities are in units of 10^3 DN s^{-1} . The spatially integrated GOES 1–8 Å light curve is also shown.

has the clearest signatures, a GOES B-class flare observed on February 1, 2007 near 15:45 UT. The stack plots and light curves from this event are shown in Figure 3. Data from only 6 of the 20 available EIS spectral windows are given. There is a clear progression in the time of the peak emission from the XRT Al_{poly} to the EIS Si X. At the lower temperatures the signature of the event is not as clear, suggesting some contamination from foreground and background emission. The Si VII

light curve is particularly difficult to understand. The emission in this line peaks very early, before a significant rise in the high temperature light curves and there is very little emission in Si VII during the decay of the event.

To aid in the interpretation of these light curves we have also assembled some images of this event, which are shown in Figure 4. In addition to the XRT Al_{poly}/Open and Al_{poly}/Al_{thick} images we show the STEREO B EUVI

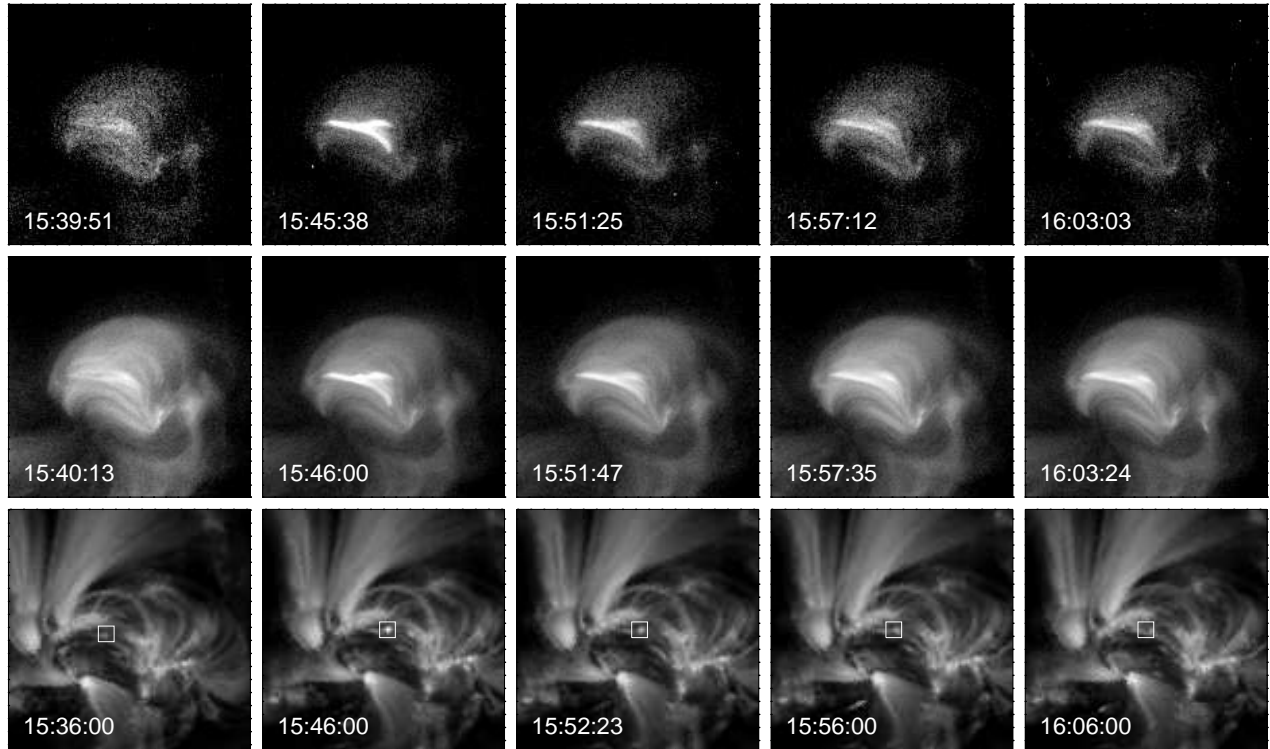


Fig. 4. XRT (Al-poly/Open and Al-poly/Al-thick) and STEREO B EIVI 171 Å images for the B flare observed on February 1, 2007 near 15:45. The spatial position of the footpoint spectra shown in Figure 5 is indicated by the box. A movie is provided as on-line material.

Fe IX/X 171 Å images from this time (Howard et al. 2002). There are no TRACE images during the event because the spacecraft was experiencing an orbital eclipse. These images indicate how complex even a small transient event can be. The XRT images show that the emission at high temperatures does not come from a single loop but several loops. The 171 Å images show an intense footpoint brightening, suggesting that the spike in the Si VII emission originates in one of the loop footpoints.

The appearance of the loop in the XRT Al-thick filter suggests that the emission reaches very high temperatures. We have found signatures of this high temperature emission in the EIS spectra. The Fe XXIV 255.1 and 192.0 Å lines appear very briefly in these data, peaking at about 15:45, coincident with the peak in the GOES 1–8 Å flux. At this time Fe XXIII 263.76 Å also appears. During this event emission at Fe XVII 254.87 Å and Ca XVII 192.87 Å are also observed. For this relatively weak event, the Ca XVII emission is difficult to disentangle from the Fe XI and O V blends.

The footpoint emission observed at the lower temperatures (such as Si VII) have an interesting Doppler signature. Profiles near to the top of the brightening show a significant shift relative to profiles at the bottom of the brightening. This phenomenon in the Si VII profile is illustrated in Figure 5. Here the profile +2'' from the center of the footpoint is blueshifted by about 30 km s⁻¹, but is approximately Gaussian. The profile -2'' from the center shows only a small shift in the peak, but the profile is broadened out beyond 100 km s⁻¹. This behavior suggestive of the bi-direction jets observed in transition region

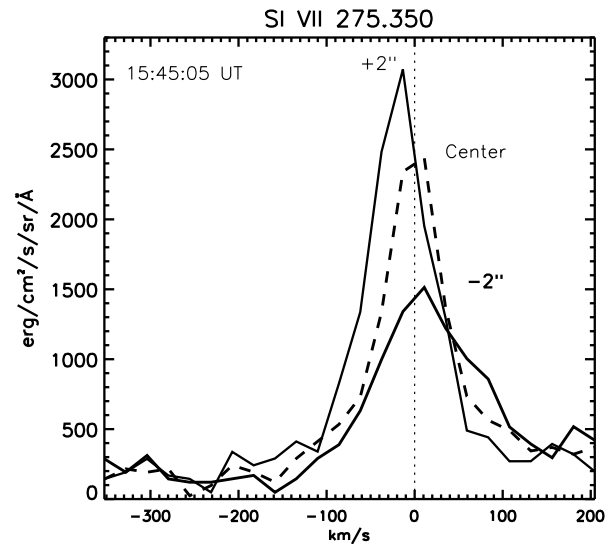


Fig. 5. Line profiles from Si VII 275.35 Å in one of the loop footpoints. The line profiles away from the center of the brightening show relative Doppler shifts suggesting to formation of a reconnection jet.

emission lines with the SUMER spectrometer on SOHO. These bi-directional flows have been interpreted as evidence for magnetic reconnection (Innes et al. 1997).

The emission observed at the higher temperatures with EIS does not appear to show significant Doppler signatures. The line centroids are generally within a few km s⁻¹ of their pre-

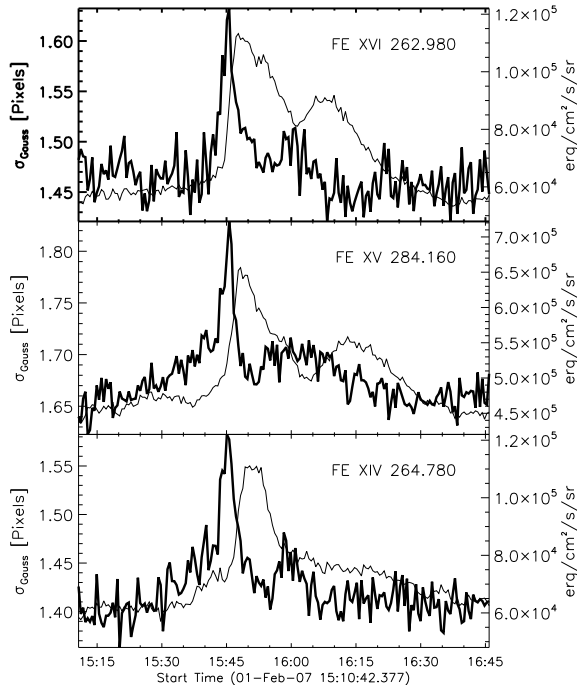


Fig. 6. The evolution of the line width σ_{Gauss} (thick line) and intensity (thin line) for Fe XVI 262.98 Å, Fe XV 285.15 Å, and Fe XIV 264.78 Å. The line widths peak before the peak in the line intensity.

flare positions. The line widths, in contrast do show some interesting behavior during the heating event. As illustrated in Figure 6, the line widths for Fe XVI, Fe XV, and Fe XIV peak during the rise phase in the event. In all of the lines, the peak in the line width is achieved before the peak in the line intensity. A similar behavior is often observed in flares, where the peak non-thermal velocity typically occurs at or before the peak in intensity (Alexander et al. 1998; Mariska & McTiernan 1999). In the flare case it has been conjectured that this is related to turbulent motions during the heating. Since the plasma observed in these emission lines is presumably cooling, the origin of the excess width early in the event is difficult to interpret.

5. Discussion

We have presented an initial look at active region transient brightenings observed with the EIS and XRT instruments on Hinode. The high spatial and temporal resolution of these instruments indicate that high temperature active region emission can be highly dynamic, suggesting that impulsive heating is more important than previously thought. The fine temperature resolution of EIS allows us to follow the evolution of active region plasma in great detail. We see numerous examples of plasma cooling from high temperatures to lower temperatures and have presented one example in some detail. To our knowledge this is the most complete observation of an active region transient to date. The very broad temperature coverage of EIS allows us to follow the temperature evolution from above 10 MK to below 0.1 MK. The high spectral resolution of EIS also allows us to identify possible velocity signatures of active region heating in one event. We find what appear to be bi-directional flows at the loop footpoints and excess line

widths during the rise phase of the event.

These results, however, are preliminary. They generally come from the analysis of a single event from a single active region. Our impression is that this event is qualitatively similar to the other, smaller events that are observed in this region. Many more systematic studies of active region transient activity with Hinode are clearly required.

While the analysis of transient events observed with XRT and EIS has the potential to yield insights into the coronal heating mechanism, it is also possible that there is a strong steady heating level that contributes to the active region heating. The light curves presented in Figure 2 clearly show a high basal level of several thousand DN s^{-1} . Differentiating between steady heating with transient events superimposed and purely impulsive heating will require detailed statistical analysis and modeling of the observed light curves (e.g., Shimizu et al. 1992).

The heating of the solar corona is undoubtedly related to the evolution of surface magnetic fields and incorporating the analysis of magnetic field data and chromospheric emission from the SOT on Hinode is also very important. We have surveyed the SOT data from this period and we see a wealth of activity at these heights in the solar atmosphere. Much of the photospheric flux, however, closes before it reaches the corona (Close et al. 2003) so the challenge is to determine what activity is relevant to the coronal dynamics we observe.

Hinode is a Japanese mission developed and launched by ISAS/JAXA, with NAOJ as domestic partner and NASA and STFC (UK) as international partners. It is operated by these agencies in co-operation with ESA and NSC (Norway). We thank Spiros Patsourakos for preparing the STEREO EUVI data for us. We also thank the referee for a thorough reading of the manuscript and many insightful comments.

References

- Alexander, D., Harra-Murnion, L. K., Khan, J. I., & Matthews, S. A. 1998, *ApJL*, 494, L235
- Aschwanden, M. J., Schrijver, C. J., & Alexander, D. 2001, *ApJ*, 550, 1036
- Brooks, D. H., & Warren, H. P. 2007, *ApJ*, submitted
- Cargill, P. J., Mariska, J. T., & Antiochos, S. K. 1995, *ApJ*, 439, 1034
- Close, R. M., Parnell, C. E., Mackay, D. H., & Priest, E. R. 2003, *Sol. Phys.*, 212, 251
- Culhane et al., 2007, *Sol. Phys.*, in press
- Golub et al., 2007, *Sol. Phys.*, in press
- Howard, R. A., Moses, J. D., Socker, D. G., Dere, K. P., and Cook, J. W., 2002, *Advances in Space Research*, 29, 2017
- Innes, D. E., Inhester, B., Axford, W. I., & Wilhelm, K. 1997, *Nature*, 386, 811
- Kano, R., & Tsuneta, S. 1996, *PASJ*, 48, 535
- Kosugi et al., 2007, *Sol. Phys.*, in press
- Lenz, D. D., Deluca, E. E., Golub, L., Rosner, R., & Bookbinder, J. A. 1999, *ApJL*, 517, L155
- Mariska, J. T., & McTiernan, J. M. 1999, *ApJ*, 514, 484
- Porter, L. J., & Klimchuk, J. A. 1995, *ApJ*, 454, 499
- Rosner, R., Tucker, W. H., & Vaiana, G. S. 1978, *ApJ*, 220, 643
- Schrijver, C. J., Sandman, A. W., Aschwanden, M. J., & DeRosa, M. L. 2004, *ApJ*, 615, 512
- Shimizu, T. 1995, *PASJ*, 47, 251

- Shimizu, T., Tsuneta, S., Acton, L. W., Lemen, J. R., & Uchida, Y.
1992, PASJ, 44, L147
- Ugarte-Urra, I., Winebarger, A. R., & Warren, H. P. 2006, ApJ, 643,
1245
- Warren, H. P., & Winebarger, A. R. 2006, ApJ, 645, 711
- Warren, H. P., Winebarger, A. R., & Hamilton, P. S. 2002, ApJL, 579,
L41
- Warren, H. P., Winebarger, A. R., & Mariska, J. T. 2003, ApJ, 593,
1174
- Winebarger, A. R., Warren, H. P., & Mariska, J. T. 2003, ApJ, 587,
439
- Winebarger, A. R., & Warren, H. P. 2005, ApJ, 626, 543